Applied Catalysis B: Environmental 327 (2023) 122471

Contents lists available at ScienceDirect

Applied Catalysis B: Environmental

journal homepage: www.elsevier.com/locate/apcatb

Highly efficient and stable photothermal catalytic CO_2 hydrogenation to methanol over Ru/In_2O_3 under atmospheric pressure

Bowen Deng [a,b], Hui Song [a,*], Qi Wang [a,b], Jianan Hong [d], Shuang Song [a,e], Yanwei Zhang [d], Kang Peng [a,f], Hongwei Zhang [g], Tetsuya Kako [a], Jinhua Ye [a,b,c,**]

[a] International Center for Materials Nanoarchitectonics (WPI-MANA), National Institute for Materials Science (NIMS), 1–1 Namiki, Tsukuba, Ibaraki 305–0044, Japan
[b] Graduate School of Chemical Sciences and Engineering, Hokkaido University, Sapporo 060–0814, Japan
[c] TJU-NIMS International Collaboration Laboratory, School of Material Science and Engineering, Tianjin University, Tianjin 300072, PR China
[d] State Key Laboratory of Clean Energy Utilization, Zhejiang University, Hangzhou 310027, PR China
[e] Institute of Fundamental and Frontier Sciences, University of Electronic Science and Technology of China, Chengdu 611731, PR China
[f] State Key Laboratory for Mechanical Behavior of Materials, Xi'an Jiaotong University, Xi'an 710049, PR China
[g] Biogas Institute of Ministry of Agriculture and Rural Affairs, Chengdu 610041, PR China

ARTICLE INFO

Keywords:
CO_2 hydrogenation
Methanol
Photothermal catalysis
Indium oxide
Ruthenium

ABSTRACT

Photothermal catalytic CO_2 hydrogenation to CH_3OH with renewable H_2 is a promising method to convert solar energy into chemical energy. However, it is still impeded by limited CO_2 conversion efficiency and poor CH_3OH selectivity under mild conditions. Herein, we report a Ru/In_2O_3 catalyst for efficient and stable photothermal CH_3OH production from CO_2 hydrogenation under atmospheric pressure. The Ru/In_2O_3 catalyst delivers a remarkable solar CH_3OH production of 280.4 μmol g^{-1} h^{-1}, which is ~50 times higher than that of pure In_2O_3 under the same conditions and surpasses by far reported In_2O_3-based photothermal catalysts. Detailed characterizations demonstrate that the synergy of photothermal heating effect and hot-carriers-induced activation of reactants on Ru together with the interaction between Ru and In_2O_3 enhances the activation of CO_2 and H_2. Moreover, Ru modulates the electronic structure of In_2O_3 and promotes the generation of oxygen vacancies, which is favorable for the hydrogenation process to form CH_3OH. This work paves a way for the rational design of efficient catalysts for solar CH_3OH production from CO_2 hydrogenation under mild conditions.

1. Introduction

The development of modern society has accelerated the consumption of non-renewable fossil fuel energy, resulting in multiple energy crises and environmental problems[1,2]. Methanol (CH_3OH) is an essential chemical industrial feedstock and also considered as a promising candidate for clean and renewable energy carriers due to its high volume-specific energy density[3]. Nowadays, fossil fuels conversion domains the process of industrial methanol production, resulting in massive energy consumption and immense CO_2 emission. Methanol production from CO_2 hydrogenation is regarded as a sustainable and environmental-friendly route and has attracted worldwide interest [4–6].

Over the past several decades, many efforts have been taken to realize efficient thermocatalytic CO_2 hydrogenation to methanol, mostly using Cu-based nanocomposites as catalysts[7–9]. However, due to the exothermic characteristics of methanol synthesis (Eq. (1)) and the competing CO production via side reverse water-gas shift reaction (RWGS, Eq. (2)), this process demands relatively harsh reaction conditions, especially an ultrahigh pressure (temperature of 200 ~ 300 °C and pressure of 3 ~ 10 Mpa), to simultaneously achieve high methanol selectivity and production rate, which results in excess energy consumption, thereby hindering the large-scale industrial application[10,11].

$$CO_2 + 3\ H_2 \Leftrightarrow CH_3OH + H_2O,\ \Delta H^\circ_{298\ K} = -49{\cdot}5\ kJ\ mol^{-1} \quad (1)$$

$$CO_2 + H_2 \Leftrightarrow CO + H_2O,\ \Delta H^\circ_{298\ K} = +41{\cdot}2\ kJ\ mol^{-1} \quad (2)$$

* Corresponding author.
** Corresponding author at: International Center for Materials Nanoarchitectonics (WPI-MANA), National Institute for Materials Science (NIMS), 1–1 Namiki, Tsukuba, Ibaraki 305–0044, Japan.
E-mail addresses: SONG.Hui@nims.go.jp (H. Song), Jinhua.YE@nims.go.jp (J. Ye).

https://doi.org/10.1016/j.apcatb.2023.122471
Received 16 November 2022; Received in revised form 9 January 2023; Accepted 12 February 2023
Available online 13 February 2023

Recently, photothermal catalysis based on plasmonic nanometals composites has attracted great interest due to its promising prospect in the field of fuel production and fine chemical conversion, together with the utilization of clean and regenerable solar energy, which is regarded as an ideal energy source for future human society[12–15]. The light-induced hot carriers are capable to activate chemical bonds and trigger reaction processes, such as the dissociation of H_2 and the activation of C═O bond[16–19]. Therefore, it is expected to be a promising technology to catalyze CO_2 hydrogenation to methanol via photothermal process, also known as "solar methanol production", which could convert solar energy into valuable chemical energy as fuel and industrial feedstock without extra greenhouse gas generation[20]. However, quite few studies have been reported on photothermal methanol production under mild conditions, especially at ambient pressure[21–23]. Among these studies, both activity and selectivity are still relatively low, inhibiting the further application of photothermal methanol production from CO_2 hydrogenation, and the detailed mechanism still requires thorough investigation and discussion[24,25].

In_2O_3 has been demonstrated to be an excellent catalyst for CO_2 hydrogenation to CH_3OH according to recent reported works, including thermal catalysis, photocatalysis and photothermal catalysis[22,26]. The oxygen vacancies (V_o) in In_2O_3 play a key role in modulating the catalytic activity of methanol production in CO_2 hydrogenation[27–29]. Furthermore, transition metals including noble metals (Pd, Pt, Rh, Au) and non-noble metals (Ni, Co) have been utilized to modify the surface chemical architectures of In_2O_3 and provide active sites for CO_2 and H_2 activation, thereby contributing to enhanced catalytic performance [30–33]. However, most related researches are focused on the thermal catalytic process under high pressure (usually 1.0 MPa ~ 5.0 MPa), thus rendering such composites potential candidates for solar methanol production under mild conditions.

Herein, Ru-loaded In_2O_3 nanorods were synthesized for photothermal methanol production from CO_2 hydrogenation under atmospheric pressure. Upon light irradiation, a maximum methanol production of 280.4 μmol g^{-1} h^{-1} was obtained over 2 wt% Ru/In_2O_3, which was around 50 times higher than that of pure In_2O_3. Mechanism investigation demonstrated that the outstanding catalytic activity was assigned to the interfacial interaction between Ru and In_2O_3, the improved concentration of oxygen vacancies by loading Ru, as well as the photo-thermal synergistic effect on CO_2 hydrogenation. Detailed studies and DFT calculations suggested that methanol was mainly produced via the CO-hydrogenation route, in which Ru nanoparticles facilitated the activation and conversion of H_2 and CO_2 assisted by light-induced hot carriers, and afterwards the oxygen vacancies on In_2O_3 favored the hydrogenation process from absorbed intermediates *CO to final product methanol.

2. Experimental section

2.1. Materials

All chemicals were utilized without any treatment. Indium (III) chloride ($InCl_3$), rhodium (III) chloride ($RhCl_3$), ruthenium (III) chloride ($RuCl_3$), hexachloroplatinic acid (H_2PtCl_6), palladium (II) chloride ($PdCl_2$), copper (II) nitrate trihydrate ($Cu(NO_3)_2{\cdot}3\ H_2O$), aluminum(III) nitrate nonahydrate ($Al(NO_3)_3{\cdot}9\ H_2O$), zinc(II) nitrate hexahydrate ($Zn(NO_3)_2{\cdot}6\ H_2O$), sodium carbonate (Na_2CO_3), urea, Sodium borohydride ($NaBH_4$), commercial In_2O_3 were purchased from Wako Chemical Co., Ltd. Distilled water (18.2 MΩ cm) was utilized in this work.

2.2. Catalyst preparation

2.2.1. Synthesis of In_2O_3

In_2O_3 was synthesized based on a reported hydrothermal method [34]. Specifically, 0.29 g $InCl_3$ and 1.2 g urea were dissolved into 80 mL of deionized water, and the solution was continuously stirred at room temperature for 1 h. Then the transparent solution was transferred into a 100 mL Teflon-lined stainless-steel autoclave and maintained at 140 °C for 12 h. After cooling to room temperature, the white sediments in the autoclave were centrifugated and washed by distilled water several times, then dried in a vacuum oven at 70 °C overnight. Afterwards, the white precursors were calcinated in air at 250 °C for 4 h with a ramping rate of 5 °C min^{-1} to obtain In_2O_3 powder.

2.2.2. Synthesis of nanometals/In_2O_3

Metal nanoparticles (Ru, Rh, Pt, Pd, Cu) were loaded on the synthesized In_2O_3 using $NaBH_4$ as a reducing agent. Specifically, for 2 wt% Ru/In_2O_3, 200 mg In_2O_3 and 8.2 mg $RuCl_3$ were dissolved into 100 mL deionized water under vigorous stirring for 1 h. Then a fresh $NaBH_4$ solution (100 mM, 10 mL) was introduced drop by drop to reduce Ru^{3+}. Afterwards, the sample was filtered and washed with water for 6 times, and then dried overnight in a vacuum oven at 70 °C. For different loading amount (0.5 wt%, 1.0 wt%, 5.0 wt%), the amount of $RuCl_3$ was changed to 2.1, 4.1 and 20.5 mg respectively. Rh/In_2O_3, Pt/In_2O_3, Pd/In_2O_3 and Cu/In_2O_3 were produced by the same procedure except using corresponding metal precursors ($RhCl_3$, H_2PtCl_6, H_2PdCl_6, $Cu(NO_3)_2{\cdot}6\ H_2O$).

2.2.3. Synthesis of reference catalysts

CuZnAl was synthesized using the co-precipitation method as described in previous work[35]. Reference catalyst ($2Ru/com\text{-}In_2O_3$) was synthesized by the same method as Ru/In_2O_3 except for the commercial In_2O_3 instead of synthesized In_2O_3. Another reference catalyst ($2Ru/In_2O_3$-wet) was synthesized by the wet-impregnation method. A certain amount of $RuCl_3$ solution was impregnated on synthesized In_2O_3 followed by annealing at 250 °C for 2 h in air.

2.3. Characterization

A PANalytical B.V. XRD diffractometer with Cu Kα radiation (λ = 1.5406 Å) was utilized to obtain the powder X-ray diffraction (XRD) results. The contents of Ru and In in samples were analyzed via inductively coupled plasma-optical emission spectrometry (ICP-OES, Agilent 720-ES). A JEOL JEM-F200 (HR) transmission electron microscopy operated at 200 kV was utilized to collect the transmission electron micrography (TEM) and high-resolution TEM (HRTEM) images of catalysts. The elemental distribution of samples was recorded through energy-dispersive X-ray spectroscopy (EDS) test on the above TEM equipment. The AutoChem II 2920 chemisorption equipment was used to carry out H_2-TPR test. The Thermo Fisher ESCALAB Xi+ system was utilized to collect X-ray photoelectron spectroscopy (XPS) of samples. A Shimadzu UV-2500 spectrometer with an integrating sphere accessory was used to obtain the UV-Visible diffuse reflectance spectroscopy (UV-Vis DRS). Raman spectroscopy was collected on the Raman microscope (NRS-1000, Japan) equipped with a green laser (532 nm) as the excitation source. Indium K-edge X-ray absorption near edge structure (XANES) spectra were measured at the Photon Factory Advanced Ring in Tsukuba, Japan.

2.4. Catalytic performance evaluation

Solar-driven photothermal catalytic CO_2 hydrogenation experiment was carried out in a homemade quartz reactor, which has been described in our previous work[35]. 300 W Xenon arc lamp equipped with an L42 filter was utilized as the illuminant and the only energy input. A Thorlabs PM-100D optical power meter with an S401C sensor was utilized to measure the intensity of. During the experiment, 10 mg catalyst was smoothly dispersed onto an air-permeable quartz fiber filter in the reactor. A thermocouple located at the center of sample surface was utilized to monitor the temperature of catalyst. The mixed reaction gas (CO_2/H_2 = 1:3) flowed through the system with a rate of 20 mL min^{-1}. After purging for 0.5 h, the light was switched on to initial the

solar-driven experiment. The venting gas was injected into a gas chromatography (Shimadzu GC2014) to analyze the components. The CG was equipped with two capillary columns (porapak-Q and shincarbon-A) and a flame ionization (FID) detector.

Photo-assisted thermocatalytic CO_2 hydrogenation reaction was carried out in a flow-type stainless-steel reaction system with external electric heating, which has also been described in our previous work [35]. The catalyst temperature was controlled by a temperature controller (TC-1000 JASCO) and a thermocouple. The visible light source was an LA-251 Xe lamp with L42 and HA30 filters. Specifically, 10 mg sample was uniformly dispersed onto the sample holder. Then a gas mixture ($CO_2/H_2 = 1/3$) flowed through the reaction system with a rate of 20 mL min^{-1}. After purging for 30 min, the electrical heater was turned on to elevate the reactor temperature in a ramping rate of 5 ^oC min^{-1}. The analysis of products was the same as the above experiment.

2.5. In situ DRIFTS analysis

A JASCO FT-IR 6300 Spectrometers equipped with a liquid nitrogen-cooled mercury-cadmium-telluride (MCT) detector and an in situ diffuse reflectance cell was utilized to conduct in situ diffuse reflectance infrared Fourier transform spectroscopy (DRIFTS) test. DRTFTS spectra were recorded at 4 cm^{-1} resolution with 32 scans. Before the analyses, 10 mg catalyst was purged by Ar flow for 30 min at room temperature. Then the temperature was elevated with a ramping rate of 10 ^oC min^{-1} and maintained at 200 ^oC. After the background spectrum was obtained in Ar atmosphere, the gas flow was changed into the mixture of CO_2/H_2 (5/15 mL min^{-1}) and then in situ DRIFTS experiment was performed under irradiation.

2.6. Density functional theory calculations

All density functional theory (DFT) calculations were conducted on the QUANTUM ESPRESSO package. The exchange and correlation energy were described by the Perdew-Burke-Emzerhof (PBE) and the generalized gradient approximation (GGA) functional[36]. The cutoff energy of plane-wave basis was set as 65 Ry and the Monkhorst-Pack k-point was set as 3 × 3 × 1. Energy and gradient convergences with 10^{-6} Ry and 0.001 Ry / Å were adopted in the calculations.

The In_2O_3 (111) surface was modeled with a (2 × 2) supercell from the bulk In_2O_3, according to XRD result. The surface slab contained 48 In atoms and 72 O atoms. In order to exclude any interaction between layers, the vacuum height was set as 12 Å. The defective surface (In_2O_3-O_v) was obtained by removing one oxygen atom from the surface. The Ru_4/In_2O_3-O_v model was established by loading a tetrahedral Ru_4 cluster on the defective surface In_2O_3-O_v (Fig. S17). After optimizing the model, the atoms in the bottom layer were fixed, and the rest of atoms were allowed to relax during the calculations of the reaction mechanism investigation. The relative energy of each reaction state was defined as the energy difference between the corresponding and initial states.

3. Results and discussion

3.1. Preliminary screening of metal catalysts

$In(OH)_3$ nanorods were first synthesized by a hydrothermal method and then annealed at 250 ^oC for 4 h in air to obtain In_2O_3 nanorods[34]. After that, a variety of metals (Cu, Ru, Rh, Pd, Pt) were loaded on In_2O_3 nanorods via a $NaBH_4$-reducing method with the loading amount of metal designed at 2 wt%. According to X-ray diffraction (XRD) patterns (Fig. S1), all diffraction peaks in these catalysts were ascribed to the cubic In_2O_3 phase (PDF #65–3170). No peaks belonging to loaded metals were observed, probably due to the high dispersion of metal nanoparticles in the catalysts[37]. In order to find out the optimized composites for methanol production, the synthesized metal-loaded In_2O_3 and pure In_2O_3 were used to evaluate the thermal catalytic CO_2 hydrogenation at 250 ^oC in atmospheric pressure. As shown in Fig. 1 and Table S1, pure In_2O_3 showed a methanol production rate of 29.5 μmol g^{-1} h^{-1} with a selectivity of 21.3%. The catalytic activity for methanol production was remarkably improved by loading metals (Ru, Rh, Pt and Pd), except Cu. Whereas only loading Ru can improve both the activity and selectivity of methanol, reaching 122.8 μmol g^{-1} h^{-1} and 35.2%, respectively, and loading other metals on In_2O_3 obviously reduced the selectivity of methanol. Therefore, Ru was selected as the promoter for improving the performance of In_2O_3 in photothermal catalytic CO_2 hydrogenation to methanol.

3.2. Structure and morphology characterization

We then prepared a series of Ru/In_2O_3 catalysts with different Ru amount (denoted as xRu/In_2O_3, where x is the weight percent of Ru). The exact content of Ru in the catalysts was analyzed by the ICP-OES, as shown in Table 1. The results demonstrated the consistency between the designed and real components of synthesized catalysts. Fig. S2 showed that the diffraction peaks of xRu/In_2O_3 were all ascribed to cubic In_2O_3 phase with no peaks assigned to Ru species, indicating the high dispersion of Ru on the catalysts. The size of In_2O_3 particles was calculated based on Debye-Scherrer equation. As shown in Table 1, the size of pure In_2O_3 was ~17.5 nm, while that of all Ru/In_2O_3 particles was ~ 20 nm, suggesting that the In_2O_3 nanoparticles slightly grew with the introduction of Ru species. The specific surface areas of xRu/In_2O_3 were calculated by BET method based on the N_2 adsorption-desorption study. As shown in Table 1, pure In_2O_3 exhibited a specific surface area of 82.76 m^2 g^{-1}, and the surface areas of the samples with Ru were slightly decreased. Scanning electron microscope (SEM) images (Fig. S3) displayed that both pure In_2O_3 and Ru/In_2O_3 exhibited similar rod-like structures with around 1–2 μm in length and ~200 nm in width. High resolution transmission electron microscope (HRTEM) images (Fig. 2a and b) exhibited that the lattice distance of 0.29 nm was attributed to the facet of In_2O_3 (222), and the Ru nanoparticles were also observed on the surface of In_2O_3 with a lattice distance of 0.21 nm, corresponding to the facet of Ru (101). The images showed that the catalysts were composed of In_2O_3 nanoparticles with ~20 nm in diameter (Fig. S4), in correspondence with the size calculation results from XRD. The energy-dispersive X-ray spectroscopy (EDS) elemental distribution of $2Ru/In_2O_3$, as shown in Fig. 2c-f, demonstrated that Ru was highly dispersed on the surface of In_2O_3 nanorod, confirming the presence of Ru in the catalyst. The high dispersion of Ru also explained the absence of Ru diffraction peaks in XRD result.

The chemical states of elements in the catalysts were identified by XPS analysis (Fig. 3, Fig. S5 and Fig. S6). Fig. S5 illustrated that the In3d spectra in both In_2O_3 and $2Ru/In_2O_3$ showed similar peaks, and the peak centered at 444.2 eV could be attributed to In^{3+} 3d5/2, corresponding to the abundant In-O bonds in catalysts[38]. The oxygen vacancies in catalysts could be confirmed by O1s spectra in Fig. 3b and Fig. S6. The peaks centered at 529.7 eV, 531.3 eV and 532.4 eV could be assigned to lattice oxygen, oxygen vacancy and absorbed OH, respectively[39]. We calculated the concentration of oxygen vacancies on the surface of different catalysts (Table 1). The concentration of oxygen vacancies was 24.9% in bare In_2O_3, obviously lower than that of all Ru/In_2O_3 catalysts. In addition, the concentration of oxygen vacancies on the surface of xRu/In_2O_3 catalysts was increased as the amount of Ru was elevated from 0.5 wt% to 5 wt%, indicating that Ru nanoparticles facilitated the formation of oxygen vacancies in catalysts, which implied that the oxygen vacancies played a key role during the reaction process of CO_2 hydrogenation. The Ru3d spectra showed two peaks centered at 281.8 eV and 280.6 eV (Fig. 3c), ascribed to Ru^{x+} and Ru^0 respectively, revealing that the Ru nanoparticles were partially oxidized in the catalysts, which could be attributed to the possible Ru-O bond at the interface between Ru nanoparticles and In_2O_3[40–42].

Furthermore, the interaction between Ru and In_2O_3 in Ru/In_2O_3 catalysts was studied by H_2-temperature programmed reduction (H_2-

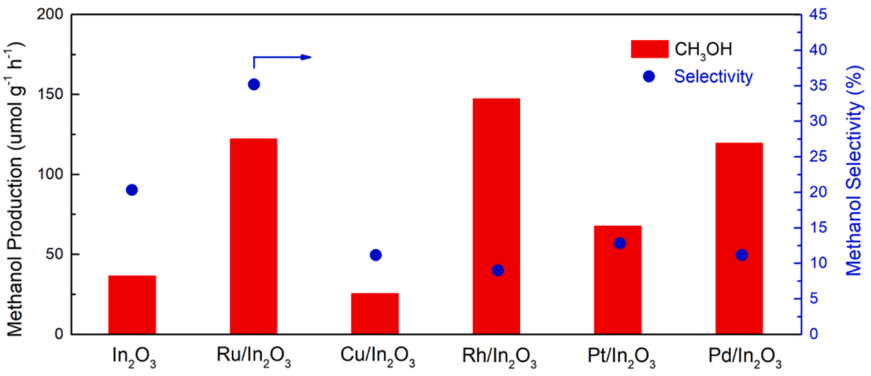

Fig. 1. Screening of metal catalysts for In_2O_3 in CO_2 hydrogenation to CH_3OH under dark conditions: 10 mg of catalyst, 250 °C, 1 bar, CO_2/H_2 = 5/15 mL min^{-1}.

Table 1
Physical and chemical properties of catalysts.

Catalysts	Ru amount (wt%)[a]	Particle size (nm)[b]	Specific surface area (m^2 g^{-1})[c]	Oxygen vacancy concentration (%)[d]
In_2O_3	0	17.5	82.76	24.9
0.5Ru/In_2O_3	0.48	20.1	79.81	32.0
1Ru/In_2O_3	0.89	20.4	76.42	35.7
2Ru/In_2O_3	1.75	21.3	77.83	38.7
5Ru/In_2O_3	4.48	21.2	78.21	46.2

[a] ICP-OES analysis,
[b] calculated by Scherrer equation using XRD data,
[c] derived from N_2 absorption-desorption study,
[d] calculated by XPS data.

TPR), and the patterns were shown in Fig. 3d. The profile of In_2O_3 exhibited a single small peak at 152 °C, which could be attributed to the formation of oxygen vacancy[43]. As for 2Ru/In_2O_3, two obvious peaks at 137 °C and 150 °C appeared in the pattern. The former peak was because of the reduction of RuO_x to metallic Ru and the latter peak was attributed to the formation of oxygen vacancies[44]. Compared with pure In_2O_3, the obviously lower temperature of oxygen vacancy formation with larger peak area suggested that the introduction of Ru in catalysts promoted the reduction of In_2O_3 through H_2 dissipation on Ru, therefore facilitating the generation of oxygen vacancies, in agreement with the XPS analysis[45].

X-ray absorption near edge structure (XANES) analysis was employed to investigate the chemical status of indium in In_2O_3 and 2Ru/In_2O_3 catalysts. As shown in the In K-edge XANES (Fig. S7), the absorption edge in 2Ru/In_2O_3 was shifted to a lower energy compared with pure In_2O_3, suggesting a lower average coordination number around In atoms, which could be attributed to the more oxygen vacancies in 2Ru/In_2O_3[46]. In addition, the Raman spectra at also demonstrated that 2Ru/In_2O_3 contained more oxygen vacancies than pure In_2O_3 (Fig. S8).

3.3. Photothermal catalytic activity measurement

The above synthesized xRu/In_2O_3 catalysts were then utilized for solar-driven photothermal catalytic CO_2 hydrogenation at atmospheric pressure. A 300 W Xenon arc lamp equipped with an L42 filter ($\lambda > 400$ nm) was utilized as the only energy source. Upon light incidence, the catalyst temperature was monitored to increase rapidly to the equilibrium temperature within 10 min (Fig. S9). As depicted in Fig. 4a, the equilibrium temperature of catalysts exhibited a linear dependence on irradiation intensity. All xRu/In_2O_3 catalysts showed much higher

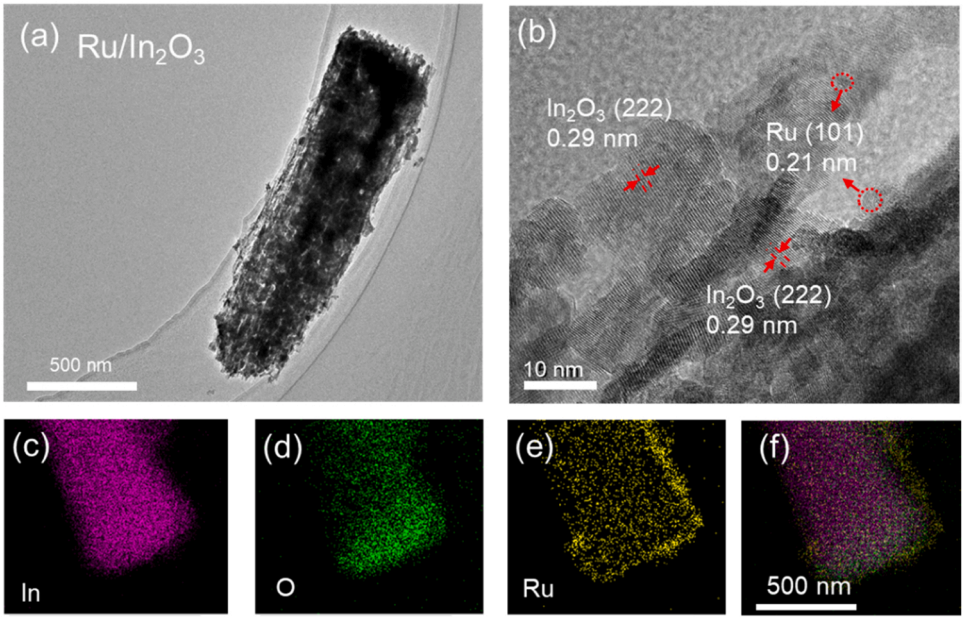

Fig. 2. Morphology of 2Ru/In_2O_3 catalyst. (a) and (b): TEM and HRTEM images, (c-f) elemental distribution spectra (EDS) of 2Ru/In_2O_3.

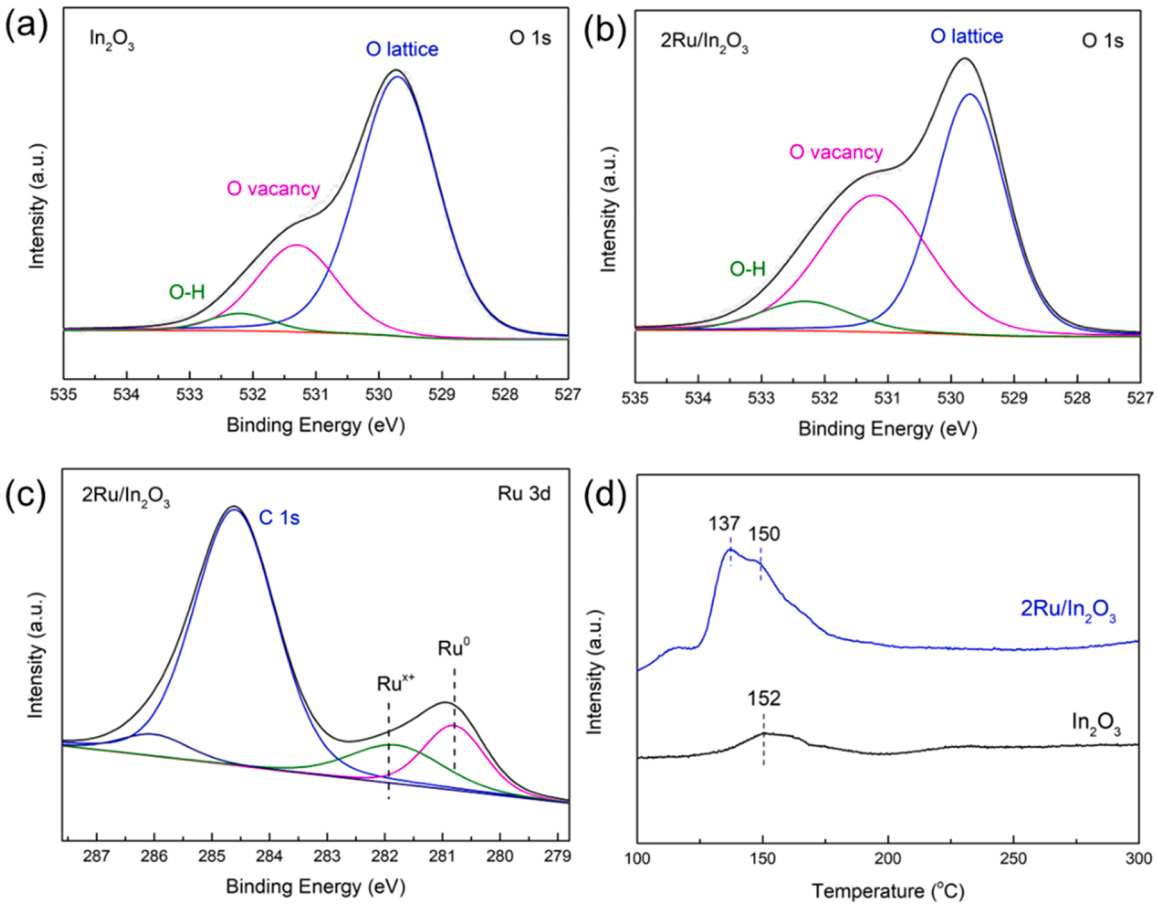

Fig. 3. Structural characterization of Ru/In_2O_3. XPS patterns for O 1s in (a) In_2O_3, (b) $2Ru/In_2O_3$ and for Ru 3d in (c) 2Ru /In_2O_3. (d) H_2-TPR patterns for In_2O_3 and $2Ru/In_2O_3$.

temperatures than that on pure In_2O_3 under the same condition, suggesting that Ru nanoparticles could absorb and convert more photon energy into phonon energy, therefore increasing the catalyst temperature. In general, only CO and methanol were detected over all catalysts in the output gas. After loading Ru on In_2O_3, both CO and CH_3OH production increased obviously, compared with pure In_2O_3 (Fig. 4b and S10). Under the light intensity of 1413 mW cm^{-2}, the optimized catalyst $2Ru/In_2O_3$ exhibited the highest methanol production (280.4 μmol g^{-1} h^{-1}), ~50 times higher than that on pure In_2O_3 catalyst (5.2 μmol g^{-1} h^{-1}). Fig. 4c showed that the methanol selectivity declined with increasing light intensity, due to the competitive endothermic RWGS reaction. It is worth noting that with the increase of Ru amount, the activity and selectivity of methanol rose at first (from 0.5 wt% Ru to 2.0 wt% Ru) and then declined (from 2.0 wt% Ru to 5.0 wt% Ru), implying that $2Ru/In_2O_3$ enhanced CH_3OH production while inhibited CO yield to some extent in comparison with other Ru/In_2O_3 catalysts, probably because of the excessive Ru covered on the surface blocking some active sites. Moreover, for comparison, we also prepared commercial methanol synthesis catalyst Cu/Zn/Al and Ru/commercial In_2O_3 (2Ru/com-In_2O_3), as well as Ru/In_2O_3 by wet impregnation method (2Ru/In_2O_3-wet). As shown in Fig. 4d, the yield and selectivity of methanol of $2Ru/In_2O_3$ in this work were much higher than those of the control catalysts. Compared with the previous works[21–23,47,48], $2Ru/In_2O_3$ exhibited an impressive solar methanol yield at atmospheric pressure (Table S2).

3.4. Light enhancement effect and reaction mechanism

Light irradiation can not only increase the surface temperature of catalysts by photothermal heating effect to promote the CO_2 hydrogenation but also potentially induces the energetic hot carriers-mediated activation of reactants to enhance the catalytic activity[49]. In order to investigate the mechanism of this photothermal process, we carried out a series of photo-assisted thermal catalytic CO_2 hydrogenation at different reaction temperatures and with or without light irradiation ($400 < \lambda < 800$ nm, 644.2 mW cm^{-2}). In this reaction process, an electrical heater with a temperature controller was equipped to alleviate the photo-induced heating effect on the catalysts. Fig. 5a and b illustrated the production rate and selectivity of methanol at 250 °C in dark and light conditions. In the dark condition, the optimized $2Ru/In_2O_3$ exhibited a methanol production much higher than that on pure In_2O_3. Upon light irradiation, the methanol yield over $2Ru/In_2O_3$ was enhanced to 178.0 μmol g^{-1} h^{-1}, promoted by nearly 50% than dark condition (122.8 μmol g^{-1} h^{-1}). Notably, there was almost no change in the methanol production over pure In_2O_3 between dark and light conditions, revealing that the visible light exhibited no effect on In_2O_3 and the light-induced enhancement in $2Ru/In_2O_3$ was mainly attributed to the Ru nanoparticles, possibly due to the coupling of light-to-heat and photo-induced hot carrier activation of reactants in Ru. Meanwhile, the selectivity of methanol remained almost no change under light irradiation, suggesting that the irradiation promoted the production of both CO and methanol.

To further study the mechanism of light-enhanced methanol production, we carried out a series of experiments on $2Ru/In_2O_3$ at different temperatures under dark and illumination. As shown in Fig. 5c, due to the exothermic property of CO_2 hydrogenation to methanol, there was a maximum production rate of methanol under dark or illumination, and the value of the maximum production rate and the corresponding reaction temperature were obviously different in these two conditions.

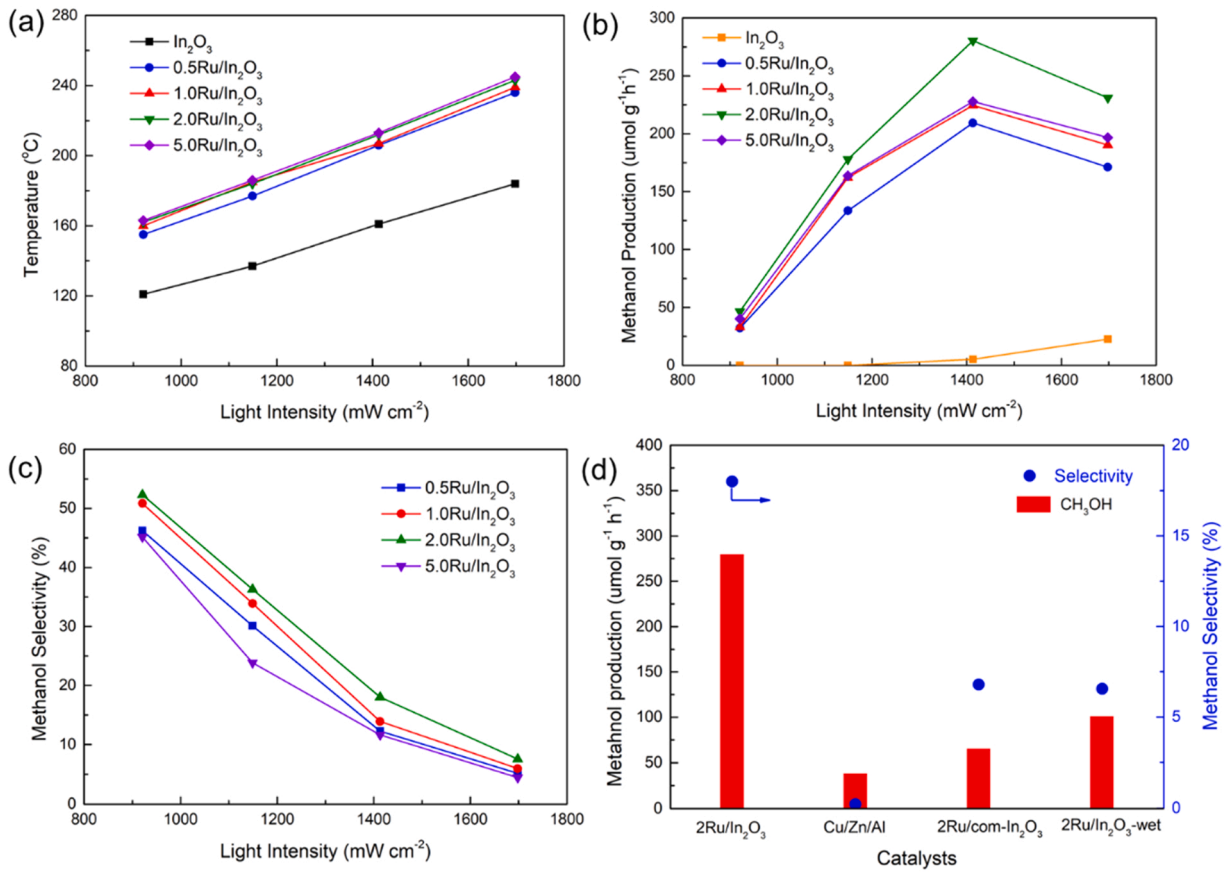

Fig. 4. Solar-driven photothermal catalytic CO_2 hydrogenation. (a) Monitored catalyst temperatures with different light intensities, (b) solar methanol generation rate and (c) selectivity over xRu/In_2O_3 catalysts, (d) comparison of methanol activity over different catalysts.

Specifically, under dark condition, the maximum production rate of methanol obtained at 290 °C was 254.9 μmol g^{-1} h^{-1}, whereas, under light irradiation, the methanol production rate reached a maximum of 290.4 μmol g^{-1} h^{-1} at 280 °C, ~20% higher than that under dark. This result demonstrated that the enhancement in the maximum methanol production rate by light was not due to the temperature elevation via solar heating, since, if so, the maximum methanol production rates under dark and illumination should be the same, but by the hot carriers-promoted methanol production over $2Ru/In_2O_3$ catalyst. In addition, when we focused on the methanol generation over pure In_2O_3 at different temperatures under dark and irradiation (Fig. 5c), the relationship between methanol activity and temperature on In_2O_3 was similar to that on $2Ru/In_2O_3$. However, there was almost no difference in production at the same temperature between dark and light conditions, indicating that the light-enhancement effect on activity over $2Ru/In_2O_3$ was mainly due to the hot carriers excited from Ru nanoparticles.

We calculated the apparent activation energy (E_a) of CO_2 reduction on $2Ru/In_2O_3$ under dark and light conditions, as shown in Fig. 5d. With the assistance of light irradiation, the E_a of CO_2 conversion on Ru/In_2O_3 decreased from 110.3 ± 4.8 kJ mol^{-1} in dark to 84.5 ± 2.7 kJ mol^{-1} under irradiation, indicating that light irradiation facilitated the reaction kinetics of CO_2 hydrogenation. In addition, the time-on-steam photothermal catalytic performances of In_2O_3 and $2Ru/In_2O_3$ were carried out at 280 °C with visible light irradiation to investigate the stability of catalysts (Fig. 5e and Fig. S11). Obviously, after 10 h reaction process, the production rate of methanol of Ru/In_2O_3 remained almost unchanged, while the methanol selectivity was gradually increased owing to the gradually decreased CO yield. After 10 h reaction, the selectivity of methanol was increased up to 23.0% over $2Ru/In_2O_3$. By contrast, the methanol production rate of In_2O_3 was decreased to only ~56% after 5 h of irradiation, indicating that the introduction of Ru significantly enhanced the stability of catalysts. Furthermore, the structure of the used catalysts showed almost no change after the long-time reaction (Fig. S12).

Fig. S13 showed that the dependence of methanol production rate on light irradiation intensity over $2Ru/In_2O_3$ exhibited a linear relationship, suggesting that the enhancement of reaction activity was driven by hot carriers induced by light irradiation[50]. In addition, the optical absorption properties of catalysts were studied by ultraviolet-visible diffuse reflectance spectroscopy (UV–vis DRS) (Fig. S14). Pure In_2O_3 mainly exhibited absorption in UV range, while all catalysts containing Ru nanoparticles showed much higher absorption in visible light range and the enhanced absorption was consistent with the deepening color of catalysts (Fig. S15), which could be mainly attributed to intra- and/or inter-band excitations of Ru nanoparticles[50]. This phenomenon indicated that the hot carriers in Ru nanoparticles were initially excited by incident photons. Then part of them dissipated rapidly to elevate the surface temperature of catalyst, while others transferred to the absorbed reactants to promote the activation of reactants CO_2 and H_2, thus enhancing the activity of methanol production, which explains the extra activity increase between thermal and photothermal methanol production in Fig. 5c.

Based on the previous reports about methanol synthesis, it has been concluded that there are mainly two pathways for CO_2 hydrogenation to methanol reaction: one is hydrocarboxyl (*COOH) intermediate for the CO hydrogenation route and the other is formate (*HCOO) intermediate for the direct CO_2 hydrogenation route[1,4,10]. In order to clarify the reaction pathway on Ru/In_2O_3, we carried out in situ diffuse reflectance infrared Fourier transform spectroscopy (DRIFTS) experiment at 200 °C and the results were shown in Fig. 6. The broad absorption area in the range from 1200 cm^{-1} to 1700 cm^{-1} was assigned to the absorption of CO_2 on catalyst surface, including CO_2^- and carbonate species[43,51,52].

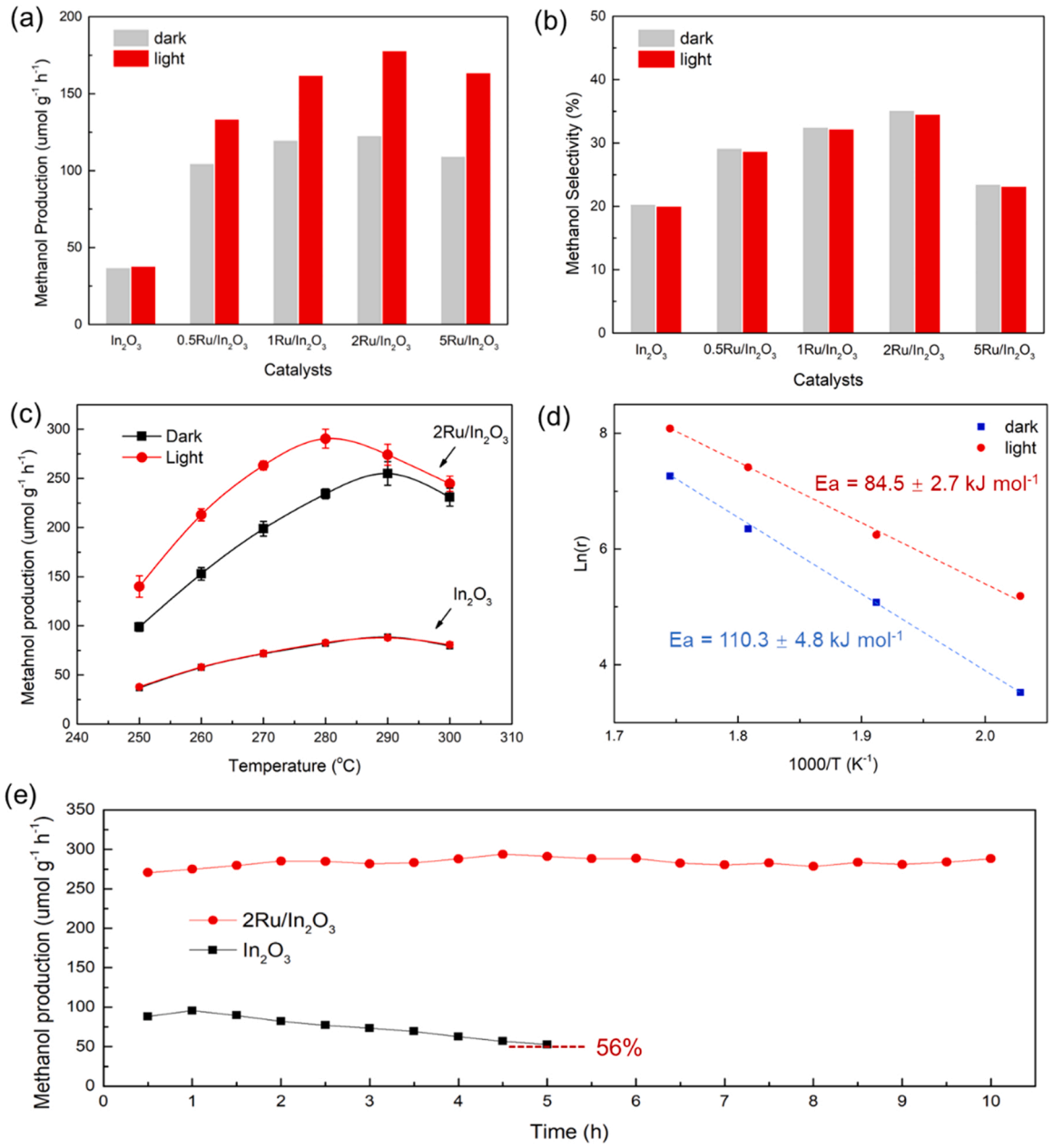

Fig. 5. Photo-assisted thermal catalytic CO_2 hydrogenation. (a) Methanol production and (b) selectivity over In_2O_3 and xRu/In_2O_3 catalysts in thermocatalytic process (dark) and photo-assisted thermocatalytic process (light) at 250 °C, (c) methanol production over In_2O_3 and $2Ru/In_2O_3$ as a function of temperature in dark and light, (d) Arrhenius plots for CO_2 conversion over $2Ru/In_2O_3$ in dark and light, (e) stability test of In_2O_3 and $2Ru/In_2O_3$ at 280 °C under the visible light irradiation. Irradiation condition: $400 < \lambda < 800$ nm, 644.2 mW cm^{-2}.

When we concentrated on the intermediate components in the reaction, the FTIR spectrum showed a peak centered at 2070 cm^{-1}, which could be attributed to CO-Ru vibration[31]. Besides, the peak centered at 1848 cm^{-1} corresponded to the stretch vibration of C═O bond in *COOH species[51,53–55]. This indicated that the reaction process on Ru/In_2O_3 followed the route of RWGS-CO hydrogenation pathway, in agreement with previous reports[56].

In order to further investigate the reaction mechanism of CO_2 hydrogenation, we conducted density functional theory (DFT) calculations about the reaction process of CO_2 hydrogenation to CH_3OH via *CO on both pure In_2O_3 and Ru/In_2O_3 surface, based on the results of in situ DRIFTS and reported studies[56]. As demonstrated in Fig. 7 and Fig. S18, the pathway of CO_2 hydrogenation on In_2O_3 and Ru/In_2O_3 could be divided into two continuous processes: (1) the dissociation of CO_2 with the assistance of spillover *H to form adsorbed *CO via a *COOH pathway; (2) the consequent hydrogenation of *CO on catalyst surface to form methanol as final product. As shown in Fig. 7, the overall process over Ru/In_2O_3 exhibited an obvious decrease in reaction state energy compared with that over pure In_2O_3, suggesting that the reaction process was more favorable on Ru/In_2O_3 surface. For process (1), the detailed calculation results about CO_2 and H_2 dissociation showed that on In_2O_3-O_v catalyst, the formation of *COOH was thermodynamically unfavorable due to the high reaction energy ($\Delta E = 1.78$ eV). In contrast, the introduction of Ru nanoparticles significantly decreased this reaction energy to 0.46 eV, therefore improving *CO generation, the important intermediate for CO_2 conversion. As for process (2), the hydrogenation process also showed a decreased energy with the assistance of Ru. As analyzed above, the oxygen vacancies (O_v) on In_2O_3 surface also participated in the reaction process of CO_2 hydrogenation to methanol, usually as the absorption sites of oxygenate species. In this

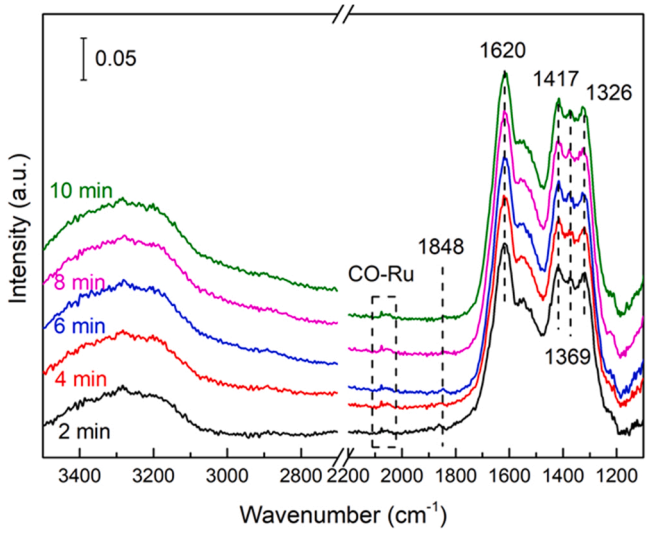

Fig. 6. In situ DRIFTS for CO_2 hydrogenation process over $2Ru/In_2O_3$ at 200 °C.

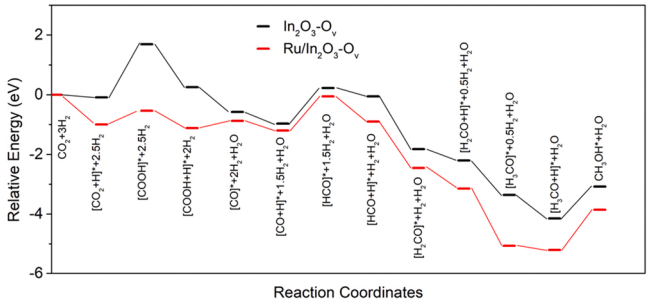

Fig. 7. Energy profiles for methanol synthesis from CO_2 hydrogenation over In_2O_3-O_v (111) and Ru_4/In_2O_3-O_v (111) models.

case, the reaction intermediate H_xCO was absorbed at the surface oxygen vacancy site in the hydrogenation process to finally form methanol. For comparison, we also calculated the reaction energy of process (2) on Ru site instead of oxygen vacancy site (Fig. S19). Obviously, the reaction process from *HCO to CH_3OH on Ru site required $\Delta E = 0.28$ eV, much higher than that on oxygen vacancy site ($\Delta E = -2.96$ eV), suggesting that oxygen vacancies played an important role in the hydrogenation process.

On the base of the above analysis and discussion, we proposed the reaction mechanism of photothermal CH_3OH synthesis from CO_2 hydrogenation over Ru/In_2O_3 (Fig. 8). The interaction between Ru and In_2O_3 increased the generation of surface oxygen vacancies (O_v), which provided more absorption sites for CO_2. Initially, hydrogen and CO_2 were adsorbed on the Ru surface and O_v of In_2O_3, respectively. The activation and conversion of reactants were facilitated by the interaction between Ru metal and In_2O_3 support and then formed adsorbed intermediate *CO via *COOH. Moreover, with the introduction of light, the excited hot carriers in Ru nanoparticles not only increased the surface temperature by dissipation to accelerate the reaction rate, but also directly enhanced the activation of H_2 and CO_2 and the conversion of intermediates to form adsorbed *CO. On one hand, CO was prone to be adsorbed on Ru site, leading to the decrease of CO generation as product to some extent. On the other hand, the oxygen vacancies facilitated the hydrogenation of *CO to CH_3OH, increasing the formation of methanol as final product. Therefore, the process of methanol generation was promoted on Ru/In_2O_3 catalyst.

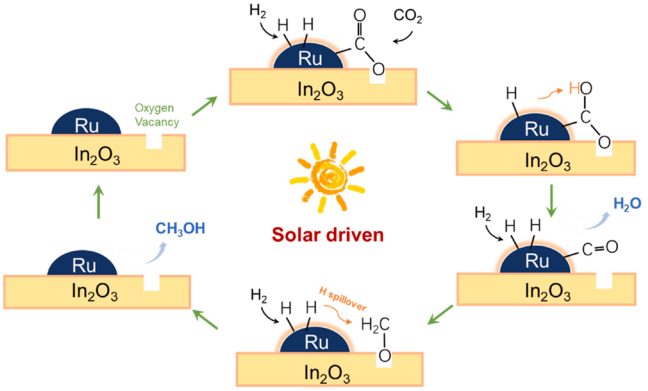

Fig. 8. Proposed mechanism for photothermal catalytic CH_3OH synthesis from CO_2 hydrogenation on Ru/In_2O_3 catalysts.

4. Conclusion

In summary, Ru/In_2O_3 catalyst was synthesized for highly efficient and stable photothermal CH_3OH production from CO_2 hydrogenation under atmospheric pressure. Under light irradiation, Ru nanoparticles not only efficiently convert solar energy into thermal energy to elevate the catalyst temperature, but also generate considerable hot carriers, which could synergistically promote the activation of adsorbed H_2 and CO_2 to form the essential intermediate *CO via *COOH. Furthermore, the generation of surface oxygen vacancies in In_2O_3 is promoted by Ru nanoparticles, which favors the consequent hydrogenation process of *CO to form final product methanol. As a result, a remarkable solar methanol production rate of 280.4 μmol g^{-1} h^{-1} was obtained over the optimized Ru/In_2O_3 catalyst. This work provides a promising strategy for photothermal methanol production via CO_2 hydrogenation under mild conditions.

Supplementary Material

Experimental results including XRD patterns, SEM and TEM figures, XPS patterns, XANES spectra, Raman spectra, activity and selectivity results, UV-Vis DRS pattern, DFT calculations.

CRediT authorship contribution statement

Bowen Deng: Conceptualization, Data curation, Formal analysis, Methodology, Validation, Investigation, Writing - original draft. **Hui Song:** Conceptualization, Investigation, Methodology, Validation, Writing - review & editing. **Qi Wang:** Investigation. **Jianan Hong:** Investigation. **Shuang Song:** Investigation, Validation. **Yanwei Zhang:** Investigation, Funding acquisition. **Kang Peng:** Investigation. **Hongwei Zhang:** Investigation. **Tetsuya Kako:** Resources. **Jinhua Ye**: Supervision, Conceptualization, Writing - review & editing, Resources, Validation, Project administration, Funding acquisition.

Declaration of Competing Interest

The authors declare that they have no known competing financial interests or personal relationships that could have appeared to influence the work reported in this paper.

Data availability

Data will be made available on request.

Acknowledgement

This work received partial financial support from Photo-excitonix

Project in Hokkaido University, JSPS KAKENHI Grant Number JP18H02065, National Natural Science Foundation of China (51976190).

Appendix A. Supporting information

Supplementary data associated with this article can be found in the online version at doi:10.1016/j.apcatb.2023.122471.

References

[1] E.C. Ra, K.Y. Kim, E.H. Kim, H. Lee, K. An, J.S. Lee, Recycling carbon dioxide through catalytic hydrogenation: recent key developments and perspectives, ACS Catal. 10 (2020) 11318–11345, https://doi.org/10.1021/acscatal.0c02930.

[2] A. Chatterjee, M.M. Gierach, A.J. Sutton, R.A. Feely, D. Crisp, A. Eldering, M. R. Gunson, C.W. O'Dell, B.B. Stephens, D.S. Schimel, Influence of El Niño on atmospheric CO_2 over the tropical Pacific Ocean: Findings from NASA's OCO-2 mission, Science 358 (2017) eaam5776, https://doi.org/10.1126/science.aam5776.

[3] A. Dhabi., Innovation Outlook: Renewable Methanol, IRENA AND METHANOL INSTITUTE, (2021) ⟨https://www.irena.org/publications/2021/Jan/Innovation-Outlook-Renewable-Methanol⟩.

[4] X. Jiang, X. Nie, X. Guo, C. Song, J.G. Chen, Recent advances in carbon dioxide hydrogenation to methanol via heterogeneous catalysis, Chem. Rev. 120 (2020) 7984–8034, https://doi.org/10.1021/acs.chemrev.9b00723.

[5] N. Podrojková, V. Sans, A. Oriňak, R. Oriňaková, Recent developments in the modelling of heterogeneous catalysts for CO_2 conversion to chemicals, ChemCatChem 12 (2020) 1802–1825, https://doi.org/10.1002/cctc.201901879.

[6] J.W. Ager, A.A. Lapkin, Chemical storage of renewable energy, Science 360 (2018) 707, https://doi.org/10.1126/science.aat7918.

[7] G. Bozzano, F. Manenti, Efficient methanol synthesis: perspectives, technologies and optimization strategies, Prog. Energy Combust. Sci. 56 (2016) 71–105, https://doi.org/10.1016/j.pecs.2016.06.001.

[8] A. García-Trenco, A. Regoutz, E.R. White, D.J. Payne, M.S.P. Shaffer, C.K. Williams, PdIn intermetallic nanoparticles for the hydrogenation of CO_2 to methanol, Appl. Catal. B 220 (2018) 9–18, https://doi.org/10.1016/j.apcatb.2017.07.069.

[9] L. Wang, E. Guan, Y. Wang, L. Wang, Z. Gong, Y. Cui, X. Meng, B.C. Gates, F. S. Xiao, Silica accelerates the selective hydrogenation of CO_2 to methanol on cobalt catalysts, Nat. Commun. 11 (2020) 1033, https://doi.org/10.1038/s41467-020-14817-9.

[10] J. Zhong, X. Yang, Z. Wu, B. Liang, Y. Huang, T. Zhang, State of the art and perspectives in heterogeneous catalysis of CO_2 hydrogenation to methanol, Chem. Soc. Rev. 49 (2020) 1385–1413, https://doi.org/10.1039/c9cs00614a.

[11] A. George, B. Shen, M. Craven, Y. Wang, D. Kang, C. Wu, X. Tu, A review of non-thermal plasma technology: a novel solution for CO_2 conversion and utilization, Renew. Sustain. Energy Rev. 135 (2021), 109702, https://doi.org/10.1016/j.rser.2020.109702.

[12] M. Ghoussoub, M. Xia, P.N. Duchesne, D. Segal, G.A. Ozin, Principles of photothermal gas-phase heterogeneous CO_2 catalysis, Energy Environ. Sci. 12 (2019) 1122–1142, https://doi.org/10.1039/c8ee02790k.

[13] Z. Wang, H. Song, H. Liu, J. Ye, Coupling of solar energy and thermal energy for carbon dioxide reduction: status and prospects, Angew. Chem. Int. Ed. 59 (2020) 8016–8035, https://doi.org/10.1002/anie.201907443.

[14] C. Xu, X. Zhang, M.-N. Zhu, L. Zhang, P.-F. Sui, R. Feng, Y. Zhang, J.-L. Luo, Accelerating photoelectric CO_2 conversion with a photothermal wavelength-dependent plasmonic local field, Appl. Catal. B 298 (2021), 120533, https://doi.org/10.1016/j.apcatb.2021.120533.

[15] M. Cai, C. Li, L. He, Enhancing photothermal CO_2 catalysis by thermal insulating substrates, Rare Met. 39 (2020) 881–886, https://doi.org/10.1007/s12598-020-01431-3.

[16] H. Song, X. Meng, T.D. Dao, W. Zhou, H. Liu, L. Shi, H. Zhang, T. Nagao, T. Kako, J. Ye, Light-enhanced carbon dioxide activation and conversion by effective plasmonic coupling effect of Pt and Au nanoparticles, ACS Appl. Mater. Interfaces 10 (2018) 408–416, https://doi.org/10.1021/acsami.7b13043.

[17] H. Robatjazi, H. Zhao, D.F. Swearer, N.J. Hogan, L. Zhou, A. Alabastri, M. J. McClain, P. Nordlander, N.J. Halas, Plasmon-induced selective carbon dioxide conversion on earth-abundant aluminum-cuprous oxide antenna-reactor nanoparticles, Nat. Commun. 8 (2017) 27, https://doi.org/10.1038/s41467-017-00055-z.

[18] G. Fu, M. Jiang, J. Liu, K. Zhang, Y. Hu, Y. Xiong, A. Tao, Z. Tie, Z. Jin, Rh/Al nanoantenna photothermal catalyst for wide-spectrum solar-driven CO_2 methanation with nearly 100% selectivity, Nano Lett. 21 (2021) 8824–8830, https://doi.org/10.1021/acs.nanolett.1c03215.

[19] S. Luo, X. Ren, H. Lin, H. Song, J. Ye, Plasmonic photothermal catalysis for solar-to-fuel conversion: current status and prospects, Chem. Sci. 12 (2021) 5701–5719, https://doi.org/10.1039/D1SC00064K.

[20] A.A. Tountas, G.A. Ozin, M.M. Sain, Solar methanol energy storage, Nat. Catal. 4 (2021) 934–942, https://doi.org/10.1038/s41929-021-00696-w.

[21] L. Wang, M. Ghoussoub, H. Wang, Y. Shao, W. Sun, A.A. Tountas, T.E. Wood, H. Li, J.Y.Y. Loh, Y. Dong, M. Xia, Y. Li, S. Wang, J. Jia, C. Qiu, C. Qian, N.P. Kherani, L. He, X. Zhang, G.A. Ozin, Photocatalytic hydrogenation of carbon dioxide with high selectivity to methanol at atmospheric pressure, Joule 2 (2018) 1369–1381, https://doi.org/10.1016/j.joule.2018.03.007.

[22] T. Yan, N. Li, L. Wang, W. Ran, P.N. Duchesne, L. Wan, N.T. Nguyen, L. Wang, M. Xia, G.A. Ozin, Bismuth atom tailoring of indium oxide surface frustrated Lewis pairs boosts heterogeneous CO_2 photocatalytic hydrogenation, Nat. Commun. 11 (2020) 6095, https://doi.org/10.1038/s41467-020-19997-y.

[23] Y. Zhao, X. Jia, G.I.N. Waterhouse, L.-Z. Wu, C.-H. Tung, D. O'Hare, T. Zhang, Layered double hydroxide nanostructured photocatalysts for renewable energy production, Adv. Energy Mater. 6 (2016), 1501974, https://doi.org/10.1002/aenm.201501974.

[24] J. Hong, C. Xu, B. Deng, Y. Gao, X. Zhu, X. Zhang, Y. Zhang, Photothermal chemistry based on solar energy: from synergistic effects to practical applications, Adv. Sci. 9 (2022), 2103926, https://doi.org/10.1002/advs.202103926.

[25] Z. Li, R. Shi, Y. Ma, J. Zhao, T. Zhang, Photodriven CO_2 hydrogenation into diverse products: recent progress and perspective, J. Phys. Chem. Lett. 13 (2022) 5291–5303, https://doi.org/10.1021/acs.jpclett.2c01159.

[26] P. Chang, Y. Wang, Y. Wang, Y. Zhu, Current trends on In_2O_3 based heterojunction photocatalytic systems in photocatalytic application, Chem. Eng. J. 450 (2022), 137804, https://doi.org/10.1016/j.cej.2022.137804.

[27] Y. Qi, L. Song, S. Ouyang, X. Liang, S. Ning, Q. Zhang, J. Ye, Photoinduced defect engineering: enhanced photothermal catalytic performance of 2D Black In_2O_{3-x} nanosheets with bifunctional oxygen vacancies, Adv. Mater. 32 (2020), e1903915, https://doi.org/10.1002/adma.201903915.

[28] L. Wang, Y. Dong, T. Yan, Z. Hu, A.A. Jelle, D.M. Meira, P.N. Duchesne, J.Y.Y. Loh, C. Qiu, E.E. Storey, Y. Xu, W. Sun, M. Ghoussoub, N.P. Kherani, A.S. Helmy, G. A. Ozin, Black indium oxide a photothermal CO_2 hydrogenation catalyst, Nat. Commun. 11 (2020) 2432, https://doi.org/10.1038/s41467-020-16336-z.

[29] W. Wei, Z. Wei, R. Li, Z. Li, R. Shi, S. Ouyang, Y. Qi, D.L. Philips, H. Yuan, Subsurface oxygen defects electronically interacting with active sites on In_2O_3 for enhanced photothermocatalytic CO_2 reduction, Nat. Commun. 13 (2022) 3199, https://doi.org/10.1038/s41467-022-30958-5.

[30] A. Bavykina, I. Yarulina, A.J. Al Abdulghani, L. Gevers, M.N. Hedhili, X. Miao, A. R. Galilea, A. Pustovarenko, A. Dikhtiarenko, A. Cadiau, A. Aguilar-Tapia, J.-L. Hazemann, S.M. Kozlov, S. Oud-Chikh, L. Cavallo, J. Gascon, Turning a methanation Co catalyst into an In–Co methanol producer, ACS Catal. 9 (2019) 6910–6918, https://doi.org/10.1021/acscatal.9b01638.

[31] M.M. Li, H. Zou, J. Zheng, T.S. Wu, T.S. Chan, Y.L. Soo, X.P. Wu, X.Q. Gong, T. Chen, K. Roy, G. Held, S.C.E. Tsang, Methanol synthesis at a wide range of H_2/CO_2 ratios over a Rh-in bimetallic catalyst, Angew. Chem. Int. Ed. 59 (2020) 16039–16046, https://doi.org/10.1002/anie.202000841.

[32] K. Sun, N. Rui, Z. Zhang, Z. Sun, Q. Ge, C.-J. Liu, A highly active Pt/In_2O_3 catalyst for CO_2 hydrogenation to methanol with enhanced stability, Green. Chem. 22 (2020) 5059–5066, https://doi.org/10.1039/d0gc01597k.

[33] J. Zhu, F. Cannizzaro, L. Liu, H. Zhang, N. Kosinov, I.A.W. Filot, J. Rabeah, A. Bruckner, E.J.M. Hensen, Ni-In synergy in CO_2 hydrogenation to methanol, ACS Catal. 11 (2021) 11371–11384, https://doi.org/10.1021/acscatal.1c03170.

[34] J. Zhao, M. Zheng, X. Lai, H. Lu, N. Li, Z. Ling, J. Cao, Preparation of mesoporous In_2O_3 nanorods via a hydrothermal-annealing method and their gas sensing properties, Mater. Lett. 75 (2012) 126–129, https://doi.org/10.1016/j.matlet.2012.01.075.

[35] B. Deng, H. Song, K. Peng, Q. Li, J. Ye, Metal-organic framework-derived Ga-Cu/CeO_2 catalyst for highly efficient photothermal catalytic CO_2 reduction, Appl. Catal. B 298 (2021), 120519, https://doi.org/10.1016/j.apcatb.2021.120519.

[36] Q. Wang, X. Ren, R. Chen, L. Jia, C. He, D. Philo, S. Li, L. Shi, S. Luo, J. Ye, Selective conversion of CO_2 to CO under visible light by modulating Cd to In ratio: a case study of Cd-In-S colloidal catalysts, Appl. Surf. Sci. 610 (2023), 155546, https://doi.org/10.1016/j.apsusc.2022.155546.

[37] J. Wang, K. Sun, X. Jia, C.-J. Liu, CO_2 hydrogenation to methanol over Rh/In_2O_3 catalyst, Catal. Today 365 (2021) 341–347, https://doi.org/10.1016/j.cattod.2020.05.020.

[38] N. Rui, F. Zhang, K. Sun, Z. Liu, W. Xu, E. Stavitski, S.D. Senanayake, J. A. Rodriguez, C. Liu, Hydrogenation of CO_2 to Methanol on a $Au^{\delta+}$–In_2O_{3-x} catalyst, ACS Catal. 10 (2020) 11307–11317, https://doi.org/10.1021/acscatal.0c02120.

[39] L. Wan, Q. Zhou, X. Wang, T.E. Wood, L. Wang, P.N. Duchesne, J. Guo, X. Yan, M. Xia, Y.F. Li, A.A. Jelle, U. Ulmer, J. Jia, T. Li, W. Sun, G.A. Ozin, Cu_2O nanocubes with mixed oxidation-state facets for (photo)catalytic hydrogenation of carbon dioxide, Nat. Catal. 2 (2019) 889–898, https://doi.org/10.1038/s41929-019-0338-z.

[40] J. Balcerzak, W. Redzynia, J. Tyczkowski, In-situ XPS analysis of oxidized and reduced plasma deposited ruthenium-based thin catalytic films, Appl. Surf. Sci. 426 (2017) 852–855, https://doi.org/10.1016/j.apsusc.2017.07.248.

[41] S. López-Rodríguez, A. Davó-Quiñonero, E. Bailón-García, D. Lozano-Castelló, F. C. Herrera, E. Pellegrin, C. Escudero, M. García-Melchor, A. Bueno-López, Elucidating the role of the metal catalyst and oxide support in the Ru/CeO_2-catalyzed CO_2 methanation mechanism, J. Phys. Chem. C. 125 (2021) 25533–25544, https://doi.org/10.1021/acs.jpcc.1c07537.

[42] K. Peng, J. Ye, H. Wang, H. Song, B. Deng, S. Song, Y. Wang, L. Zuo, J. Ye, Natural halloysite nanotubes supported Ru as highly active catalyst for photothermal catalytic CO_2 reduction, Appl. Catal. B 324 (2023), 122262, https://doi.org/10.1016/j.apcatb.2022.122262.

[43] X. Ye, C. Yang, X. Pan, J. Ma, Y. Zhang, Y. Ren, X. Liu, L. Li, Y. Huang, Highly selective hydrogenation of CO_2 to ethanol via designed bifunctional Ir_1-In_2O_3 single-atom catalyst, J. Am. Chem. Soc. 142 (2020) 19001–19005, https://doi.org/10.1021/jacs.0c08607.

[44] T.R. Garrick, W. Diao, J.M. Tengco, E.A. Stach, S.D. Senanayake, D.A. Chen, J. R. Monnier, J.W. Weidner, The effect of the surface composition of Ru-Pt bimetallic

catalysts for methanol oxidation, Electrochim. Acta 195 (2016) 106–111, https://doi.org/10.1016/j.electacta.2016.02.134.
[45] K. Shun, K. Mori, S. Masuda, N. Hashimoto, Y. Hinuma, H. Kobayashi, H. Yamashita, Revealing hydrogen spillover pathways in reducible metal oxides, Chem. Sci. 13 (2022) 8137–8147, https://doi.org/10.1039/D2SC00871H.
[46] W. Wei, Z. Wei, R. Li, Z. Li, R. Shi, S. Ouyang, Y. Qi, D.L. Philips, H. Yuan, Subsurface oxygen defects electronically interacting with active sites on In_2O_3 for enhanced photothermocatalytic CO_2 reduction, Nat. Commun. 13 (2022) 3199, https://doi.org/10.1038/s41467-022-30958-5.
[47] Z. Wang, H. Song, H. Pang, Y. Ning, T.D. Dao, Z. Wang, H. Chen, Y. Weng, Q. Fu, T. Nagao, Y. Fang, J. Ye, Photo-assisted methanol synthesis via CO_2 reduction under ambient pressure over plasmonic Cu/ZnO catalysts, Appl. Catal. B 250 (2019) 10–16, https://doi.org/10.1016/j.apcatb.2019.03.003.
[48] J. Díez-Ramírez, J.A. Díaz, P. Sánchez, F. Dorado, Optimization of the Pd/Cu ratio in Pd-Cu-Zn/SiC catalysts for the CO_2 hydrogenation to methanol at atmospheric pressure, J. CO_2 Util. 22 (2017) 71–80, https://doi.org/10.1016/j.jcou.2017.09.012.
[49] M.L. Brongersma, N.J. Halas, P. Nordlander, Plasmon-induced hot carrier science and technology, Nat. Nanotechnol. 10 (2015) 25–34, https://doi.org/10.1038/nnano.2014.311.
[50] U. Aslam, V.G. Rao, S. Chavez, S. Linic, Catalytic conversion of solar to chemical energy on plasmonic metal nanostructures, Nat. Catal. 1 (2018) 656–665, https://doi.org/10.1038/s41929-018-0138-x.
[51] N.C. Nelson, M.-T. Nguyen, V.-A. Glezakou, R. Rousseau, J. Szanyi, Carboxyl intermediate formation via an in situ-generated metastable active site during water-gas shift catalysis, Nat. Catal. 2 (2019) 916–924, https://doi.org/10.1038/s41929-019-0343-2.
[52] J. Zhao, R. Shi, G.I.N. Waterhouse, T. Zhang, Selective photothermal CO_2 reduction to CO, CH_4, alkanes, alkenes over bimetallic alloy catalysts derived from layered double hydroxide nanosheets, Nano Energy 102 (2022), 107650, https://doi.org/10.1016/j.nanoen.2022.107650.
[53] B. Moore, S.Y. Toh, Y.T.A. Wong, T. Bashiri, A. McKinnon, Y. Wai, K.W. Alethea Lee, P. Ovchinnikov, C.Y. Chiang, P. Djuricanin, T. Momose, Hydrocarboxyl radical as a product of alpha-alanine ultraviolet photolysis, J. Phys. Chem. Lett. 12 (2021) 11992–11997, https://doi.org/10.1021/acs.jpclett.1c03104.
[54] D. Forney, M.E. Jacox, W.E. Thompson, Infrared spectra of trans-HOCO, $HCOOH^+$, and HCO_2^- trapped in solid neon, J. Chem. Phys. 119 (2003) 10814–10823, https://doi.org/10.1063/1.1621382.
[55] L.O. Paulson, F.M. Mutunga, S.E. Follett, D.T. Anderson, Reactions of atomic hydrogen with formic acid and carbon monoxide in solid parahydrogen I: Anomalous effect of temperature, J. Phys. Chem. A 118 (2014) 7640–7652, https://doi.org/10.1021/jp502470j.
[56] C. Shen, K. Sun, Z. Zhang, N. Rui, X. Jia, D. Mei, C. Liu, Highly active Ir/In_2O_3 catalysts for selective hydrogenation of CO_2 to methanol: experimental and theoretical studies, ACS Catal. 11 (2021) 4036–4046, https://doi.org/10.1021/acscatal.0c05628.